

## Article

# Degradation of Landfill Leachate Using UV-TiO<sub>2</sub> Photocatalysis Combination with Aged Waste Reactors

Chunlian Wang <sup>1,2</sup>, Xiaojie Sun <sup>1,2,\*</sup>, Huijun Shan <sup>1,2</sup>, Hongxia Zhang <sup>1,2</sup> and Beidou Xi <sup>1,3,4</sup>

<sup>1</sup> Guangxi Key Laboratory of Environmental Pollution Control Theory and Technology, Guilin University of Technology, Guilin 541004, China; 1020190273@glut.edu.cn (C.W.); Secret202158@hotmail.com (H.S.); zhx75@glut.edu.cn (H.Z.); xibd@craes.org.cn (B.X.)

<sup>2</sup> Guangxi Collaborative Innovation Center for Water Pollution Control and Water Safety in Karst Area, Guilin University of Technology, Guilin 541004, China

<sup>3</sup> State Key Laboratory of Environmental Criteria and Risk Assessment, Chinese Research Academy of Environmental Sciences, Beijing 100012, China

<sup>4</sup> State Environmental Protection Key Laboratory of Simulation and Control of Groundwater Pollution, Chinese Research Academy of Environmental Sciences, Beijing 100012, China

\* Correspondence: sunxiaojie@glut.edu.cn; Tel.: +86-150-7832-9789

**Abstract:** This study explored the performance of TiO<sub>2</sub> nanoparticles in combination with aged waste reactors to treat landfill leachate. The optimum conditions for synthesis of TiO<sub>2</sub> were determined by a series of characterizations and removal rates of methyl orange. The effect of the ultraviolet irradiation time, amount of the catalyst, and pH on the removal efficiency for the chemical oxygen demand (COD) and color in the leachate was explored to determine the optimal process conditions, which were 500 min, 4 g/L and 8.88, respectively. The removal rates for COD and chroma under three optimal conditions were obtained by the single factor control method: 89% and 70%; 95.56% and 70%; and 85% and 87.5%, respectively. Under optimal process conditions, the overall average removal rates for ammonium nitrogen (NH<sub>4</sub><sup>+</sup>-N) and COD in the leachate for the combination of TiO<sub>2</sub> nanoparticles and an aged waste reactor were 98.8% and 32.5%, respectively, and the nitrate (NO<sub>3</sub><sup>-</sup>-N) and nitrite nitrogen (NO<sub>2</sub>-N) concentrations were maintained at 7–9 and 0.01–0.017 mg/L, respectively. TiO<sub>2</sub> nanoparticles before and after the photocatalytic reaction were characterized by emission scanning electron microscopy, energy dispersive spectroscopy, X-ray diffraction, and Fourier transform infrared spectrometry. In addition, TiO<sub>2</sub> nanoparticles have excellent recyclability, showing the potential of the photocatalytic/biological combined treatment of landfill leachate. This simulation of photocatalysis-landfilling could be a baseline study for the implementation of technology at the pilot scale.

**Keywords:** TiO<sub>2</sub> nanoparticles; photocatalysis; landfill leachate; aged waste reactors



**Citation:** Wang, C.; Sun, X.; Shan, H.; Zhang, H.; Xi, B. Degradation of Landfill Leachate Using UV-TiO<sub>2</sub> Photocatalysis Combination with Aged Waste Reactors. *Processes* **2021**, *9*, 946. <https://doi.org/10.3390/pr9060946>

Academic Editors: Andrea Petrella, Marco Race and Danilo Spasiano

Received: 18 April 2021

Accepted: 24 May 2021

Published: 27 May 2021

**Publisher's Note:** MDPI stays neutral with regard to jurisdictional claims in published maps and institutional affiliations.



**Copyright:** © 2021 by the authors. Licensee MDPI, Basel, Switzerland. This article is an open access article distributed under the terms and conditions of the Creative Commons Attribution (CC BY) license (<https://creativecommons.org/licenses/by/4.0/>).

## 1. Introduction

Leachates produced in landfills contain various organic and inorganic compounds, such as refractory organic material, dissolved solid particles, ammonia nitrogen (NH<sub>3</sub>-N), and heavy metals, which seriously threaten the environment and local ecosystems [1–3]. Often, combined anaerobic–aerobic biological processes can be utilized to degrade the biodegradable organic pollutants of leachates [4–6]. However, over time, the reduction of the biological oxygen demand/chemical oxygen demand (BOD<sub>5</sub>/COD) ratio < 0.3 and microorganisms involved in nitrification–denitrification processes are readily hampered by high concentrations of ammonium nitrogen, making it difficult to be treated by the conventional biological and physicochemical processes [7–10]. Moreover, additional carbon sources are needed to aid the nitrification–denitrification process [11]. Hence, a novel method has been presented to transform landfills into bioreactors via leachate recirculation, which is expected to accelerate the stabilization of landfills and reduce the organic strength

of leachates [12]. However, recirculated leachates also lead to the accumulation of higher levels of  $\text{NH}_4^+\text{-N}$  and refractory organics compared with traditional landfills because of the increasing ammonification rate and the lack of carbon sources [13].

Recently, the application of semiconductor-based photocatalysis in the treatment of landfill leachates has attracted attention [14–16]. The technology could effectively mineralize a wide range of organic pollutants into low-toxicity organic small molecules,  $\text{CO}_2$ , and  $\text{H}_2\text{O}$  without the use of expensive oxidant [17]. Among photocatalysis,  $\text{TiO}_2$  has been extensively studied due to its super strong photo-oxidizing ability, easy accessibility and environmental friendliness, and it has been considered to be a green catalyst material with broad development prospects in the field of water treatment [18,19].  $\text{TiO}_2$  absorbs UV light (<380 nm), and electrons are promoted from the valence band (VB) to the conduction band (CB) to generate electron-hole pairs ( $e^-/h^+$ ). Positive holes typically oxidize organic compounds, inducing their oxidative degradation. In addition, electrons mainly reduce molecular oxygen to superoxide radical anions, thereby leading to a number of reactive oxygen species ( $\text{OH}\cdot$ ,  $\text{O}_2^-\cdot$ , and  $\text{HO}_2\cdot$ ). Some titanium dioxide-based materials are used to treat refractory pollutants, such as prepared B- $\text{TiO}_2$ -graphene oxide ternary nanocomposite in the degradation of bisphenol A with a mineralization rate of 47.66% [20], iron-doped  $\text{TiO}_2$  photodegradation for rhodamine B at about 90% [21], and  $\text{TiO}_2$ -based catalysts obtained by different preparation methods; the simultaneous oxidation of organic matter and the reduction in ammonia were observed during the solar photocatalytic treatment of greywater [22].

Within this context, aiming to increase the effectiveness of the treatment of landfills, researchers have investigated the application of combination techniques, integrating biological processes with advanced oxidation processes [23]. Cai et al. [24] applied cetyltrimethylammonium bromide bentonite-titanium dioxide photocatalytic technology to the pretreatment of aging leachate, which maintained the removal of COD and  $\text{NH}_3\text{-N}$  at 82% and 37% in 60.02 min, respectively. Pellenz et al. [25] used a boron-doped diamond-based photo-electro-Fenton system integrated with biological oxidation to treat landfill leachate, which reduced its toxic potential. Researchers have attempted to implement anaerobic bioreactor technology for effective MSW treatment through leachate decontamination [26]. Simulations of landfilling in anaerobic bioreactors function as anaerobic sludge digesters and facilitate accelerated and economic waste stabilization [27]. The study of integrating biological processes with advanced oxidation processes in simple lab scale reactors is an important stage to enable real-scale integrated applications in the treatment of landfill leachate, which could solve the bottleneck caused by the high toxicity and insufficient carbon source of landfill leachate treatments. Thus, the main objectives of this study were two-fold. First, we intended to explore the best conditions for the synthesis of  $\text{TiO}_2$  at different hydrothermal temperatures and the different ratio of titanium to urea based on the efficiency of methyl orange and learn about optimal reaction conditions under different irradiation times, amounts of  $\text{TiO}_2$ , and initial pH regarding COD and color treatment efficiency in diluted leachate. At this stage, the  $\text{TiO}_2$  particles were characterized by energy dispersive spectrum (EDS), X-ray diffraction (XRD), and Fourier transform infrared (FTIR). The second goal was to investigate the possibility of using synthetic  $\text{TiO}_2$ -guided photocatalysis in combination with an aged waste reactor to treat landfill leachates under the best process conditions by examining the removal rates or concentration of  $\text{NH}_4^+\text{-N}$ , nitrate ( $\text{NO}_3^-\text{-N}$ ), nitrite nitrogen ( $\text{NO}_2^-\text{-N}$ ), and COD. Currently, there is relatively little published information on dealing with aging leachates by aged waste reactors combined with photocatalytic technology. This study expects to provide some suggestions for accelerating the process of waste stabilization.

## 2. Materials and Methods

### 2.1. Sampling

Landfill leachate was obtained from the Chongkou landfill in Guangxi, China. The general characteristics of the raw leachate studied were as follows: COD, 7647 mg/L; pH, 8.88;

$\text{NH}_4^+-\text{N}$ , 26.73 mg/L. The original water was diluted 30 times prior to treatment given the high contaminant load in the original landfill leachate.

Leachate samples were analyzed by the standard for pollution control on the landfill site of the MSW [28]. COD was determined in accordance with the dichromate titration method.  $\text{NH}_4^+-\text{N}$ ,  $\text{NO}_3^--\text{N}$ ,  $\text{NO}_2^--\text{N}$ , and chromaticity were measured with an ultraviolet-visible spectrophotometer (UV-6100A, Yuanxi Instrument Co., Ltd., Shanghai, China). The pH was measured using the glass electrode method (Yidian Scientific Instrument Co., Ltd., Shanghai, China) and adjusted by adding HCl or NaOH.

## 2.2. $\text{TiO}_2$ Nanoparticle Synthesis

The  $\text{TiO}_2$  nanoparticles were prepared by the green and mild solvothermal method [17,29]. First, 12.6 g of  $\text{Ti}(\text{SO}_4)_2$  and 3.15, 6.3 and 12.6 g of urea were dissolved in 40 mL of ultrapure water, the solution was stirred at room temperature for 20 min, and the mixture was transferred into a Teflon-lined stainless autoclave of 100 mL capacity, sealed, and heated at different temperatures (100 °C, 120 °C, 150 °C and 180 °C) for 12 h. After the system cooled down to room temperature, the products were washed with deionized water three times and separated by centrifugation until the system was neutral. Finally, the products were dried in air at 80 °C for 12 h. Among them, the weight ratio of  $\text{Ti}(\text{SO}_4)_2$  and urea was controlled at about 1:1, 1:2 and 1:4.

## 2.3. Characterization of $\text{TiO}_2$ Nanoparticles

Four methods of characterization were used to describe the characteristics of the synthesized  $\text{TiO}_2$  nanoparticles. To determine the structural characteristics and crystalline phases of the nanoparticles, the X-ray diffraction (XRD) method was used. The diffraction angle range of  $2\theta = 10^\circ\text{--}80^\circ$  was measured by a PANalytical X'Pert3 Powder X-ray diffractometer (the Netherlands). Field emission scanning electron microscopy (FESEM) analysis was used to visualize the morphology of the nanoparticles. This analysis was accomplished with the Electron JSM-7900F FESEM in Japan. Qualitative and quantitative analyses of the sample elements were conducted by energy dispersive spectrum (EDS) analysis and by using the electron JSM-7900F FESEM in Japan at an accelerating voltage of 15 kV. The molecular structure changes of different samples were analyzed by Fourier transform infrared spectrometry (FTIR), using a device produced in the U.S.A. by PerkinElmer, at a scan range of  $4000\text{--}400\text{ cm}^{-1}$ .

## 2.4. Photocatalytic Experiments

The visible photocatalytic activities of the obtained samples were investigated by the photodegradation of methyl orange in an aqueous solution. An amount of 20 mg of the sample was dispersed into 50 mL of the methyl orange solution (10 mg/L)/diluted leachate in a Pyrex glass reactor. A 300 W xenon lamp (Naai Precision Instrument Co., Ltd., Shanghai, China) with a UV light source (Figure 1) was used. The solution was allowed to reach an adsorption–desorption equilibrium among the photocatalyst and methyl orange by magnetic stirring in the dark for 30 min before irradiation with UV light. At certain time intervals, the 2 mL suspension was sampled and filtered through the 0.45 m filter membrane to remove the particles. The concentration of methyl orange was determined by a UV-visible spectrophotometer (UV-6100A, Yuanxi, Shanghai, China) according to its absorbance wavelength at 464 nm.

## 2.5. Cooperative Degradation Experiments

This study was conducted as a follow-up to a previous study, and the same materials were used, including anaerobic reactors formed by domestic waste (numbered C and E) and aged waste reactors (numbered D and F) (Figure 2) [13,30]. These materials were suitable for the microbial domestication of the test stage. The leachate produced by C and E was treated with D and F to form a recharge solution, which circulated back to the corresponding anaerobic landfill device. Groups CD (Figure 2a) and EF (Figure 2b)

microbially acclimatized for 14 days. The frequency obtained was 1 time/d when the leachate diluted 30 times was used as the inlet water. From day 15 to day 33, the operation mode of the CD group remained unchanged. However, in groups E and F, the effluent of reactor F was treated by the photocatalytic reactor and then recharged to reactor E. In this study, only the changes in the D and F effluent indexes were investigated.

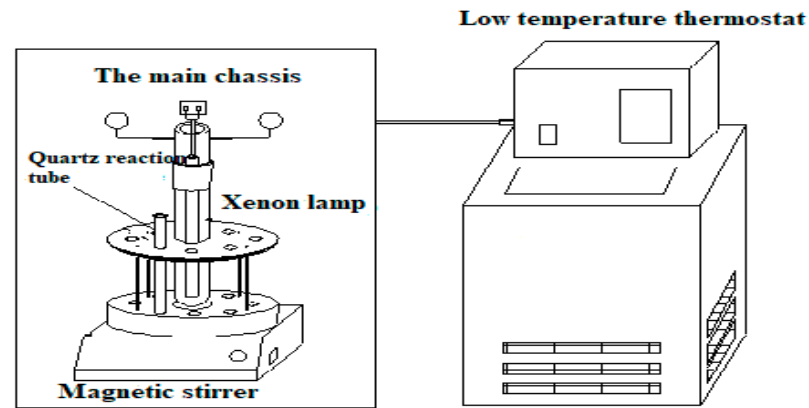


Figure 1. Schematic of the experimental setup.

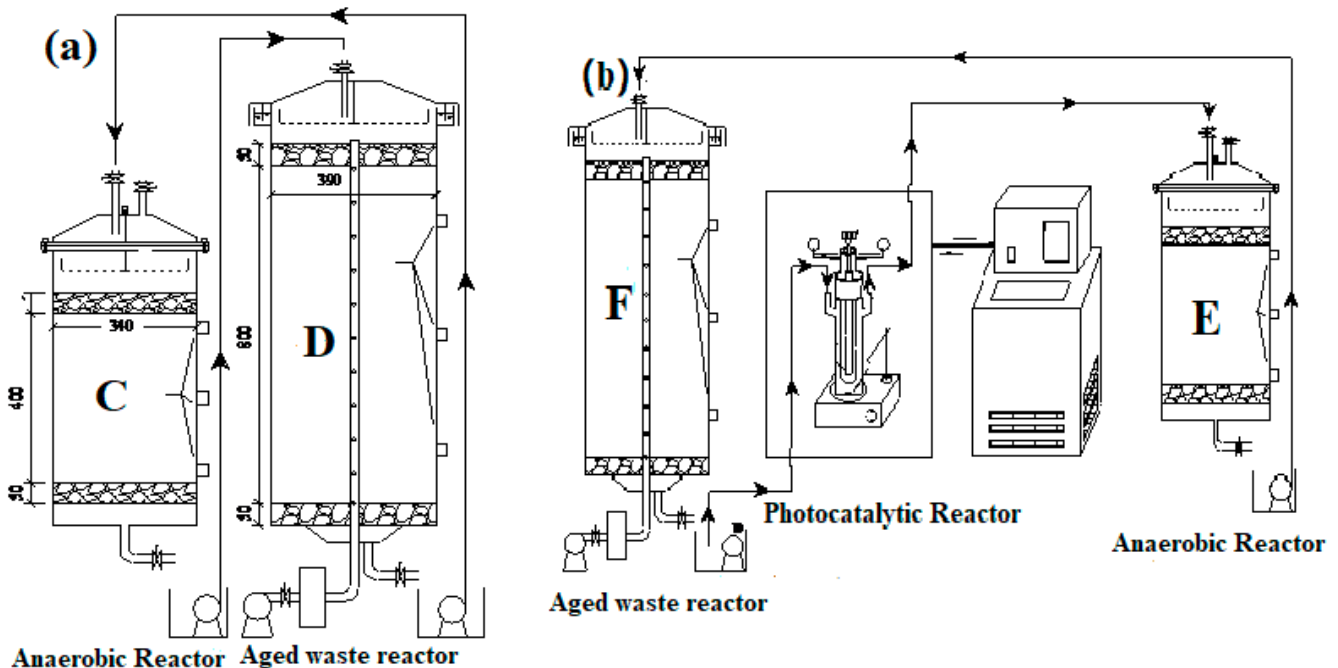


Figure 2. Schematic of bioreactor landfill (a), combined bioreactor landfill (b).

The photocatalytic reaction phase is as follows: 2 g of the  $\text{TiO}_2$  was dispersed into 500 mL (25 °C) of the effluent of reactor F with photocatalytic treatment for 8 h under simulated sunlight (500 W).

### 3. Results and Discussion

#### 3.1. Characterization of Photocatalysts

With methyl orange as the target pollutant, the best preparation conditions for  $\text{TiO}_2$  were obtained by evaluating its degradation efficiency (Figure 3). The removal ratio is calculated by the following equations [31]:

$$\text{removal ratio} = (C_0 - C)/C_0 \times 100\% \quad (1)$$

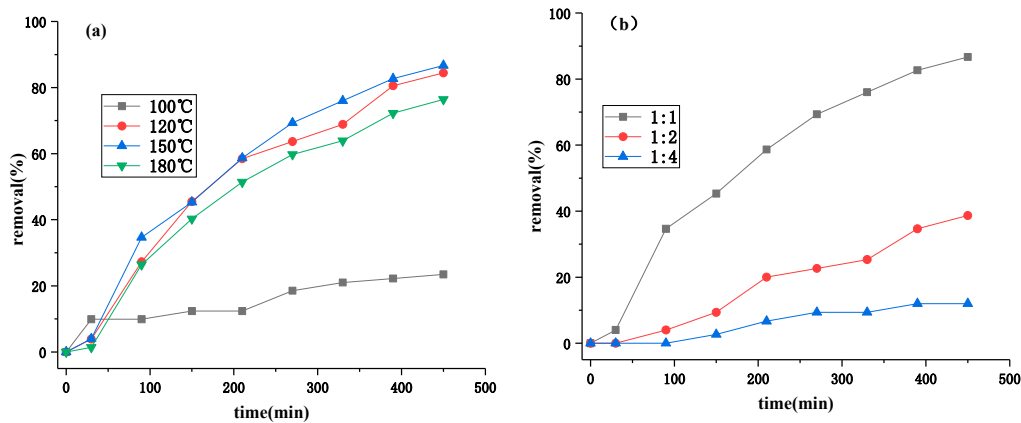


**Figure 3.** Effect of photocatalysts prepared at different temperature (a) and the different ratio of titanium to urea (b) on degradation rate of methyl orange concentration.

The surface morphology and surface area were very effective parameters in the photocatalytic activity of  $\text{TiO}_2$  [32]. The SEM images revealed that nano- $\text{TiO}_2$  had a smooth surface, and EDS analysis illustrated the content of Ti and O elements, showing that the prepared sample had high purity (Figure 4a,b). The XRD spectrum was used to analyze the crystal structure, as shown in Figure 4c,d. From data analysis, the body-centered tetragonal crystal structure of anatase was identified based on significant diffraction peaks:  $20.2^\circ$ ,  $37.8^\circ$ ,  $47.9^\circ$ ,  $53.9^\circ$ ,  $55^\circ$ , and  $62.6^\circ$  corresponding to (101), (004), (200), (105), (211), and (204) planes, respectively (JCPDS 86–1157). As previously reported in the literature, the diffraction peak of the anatase crystal form became stronger as the half-peak width narrowed, and the sample showed a good crystal form at  $150^\circ\text{C}$ . The result of the XRD patterns of products with different ratios of titanium sulfate to urea show that all the samples exhibit high crystallinity, especially when the ratio is 1:2 (Figure 4d). Meanwhile, the particle size of sample was calculated by the Scherrer formula [33]:

$$D = (K\lambda B \cos \theta) \quad (2)$$

where  $D$  is the average crystal size of the sample,  $\lambda$  is the X-ray wavelength ( $1.54056 \text{ \AA}$ ),  $B$  is the full width at half maximum of the diffraction peak (radian),  $K$  is a coefficient (0.89), and  $\theta$  is the diffraction angle at the peak maximum. The particle size of  $\text{TiO}_2$  at  $100^\circ\text{C}$ ,  $120^\circ\text{C}$ ,  $150^\circ\text{C}$ , and  $180^\circ\text{C}$  was 5.3, 9.7, 11.8, and 16.4 nm, respectively, and the particle size of  $\text{TiO}_2$  at titanium sulfate–urea ratios of 1:1, 1:2, and 1:4 was 11.8, 13.1, and 9.5 nm, respectively. Considering the crystallinity of the synthesized sample and degradation rate for methyl orange, the optimal particle size of titanium dioxide was 11.8 nm in this experiment.

The FTIR spectrum analysis chart of  $\text{TiO}_2$  prepared under controlled conditions is shown in Figure 4e,f. The characteristic peak at  $150^\circ\text{C}$  was the strongest, and the crystal structure was the most complete, which was consistent with the XRD analysis. The peak at  $460 \text{ cm}^{-1}$  of  $\text{TiO}_2$  was assigned as the Ti–O stretching vibration and Ti–O–Ti bridging stretching vibration [34]. The two signals at  $1640 \text{ cm}^{-1}$  and  $3420 \text{ cm}^{-1}$  can be ascribed to the –OH bending vibration of the water on the surface of  $\text{TiO}_2$  (Figure 4e) [35]. The adsorbed water and hydroxyl groups on the surface of the catalyst would interact with the electron-holes generated by the excitation to produce hydroxyl radicals with strong oxidizability (Figure 4e) [36]. Therefore, the best synthesis conditions are a temperature of  $150^\circ\text{C}$  and a titanium sulfate–urea ratio of 1:1.

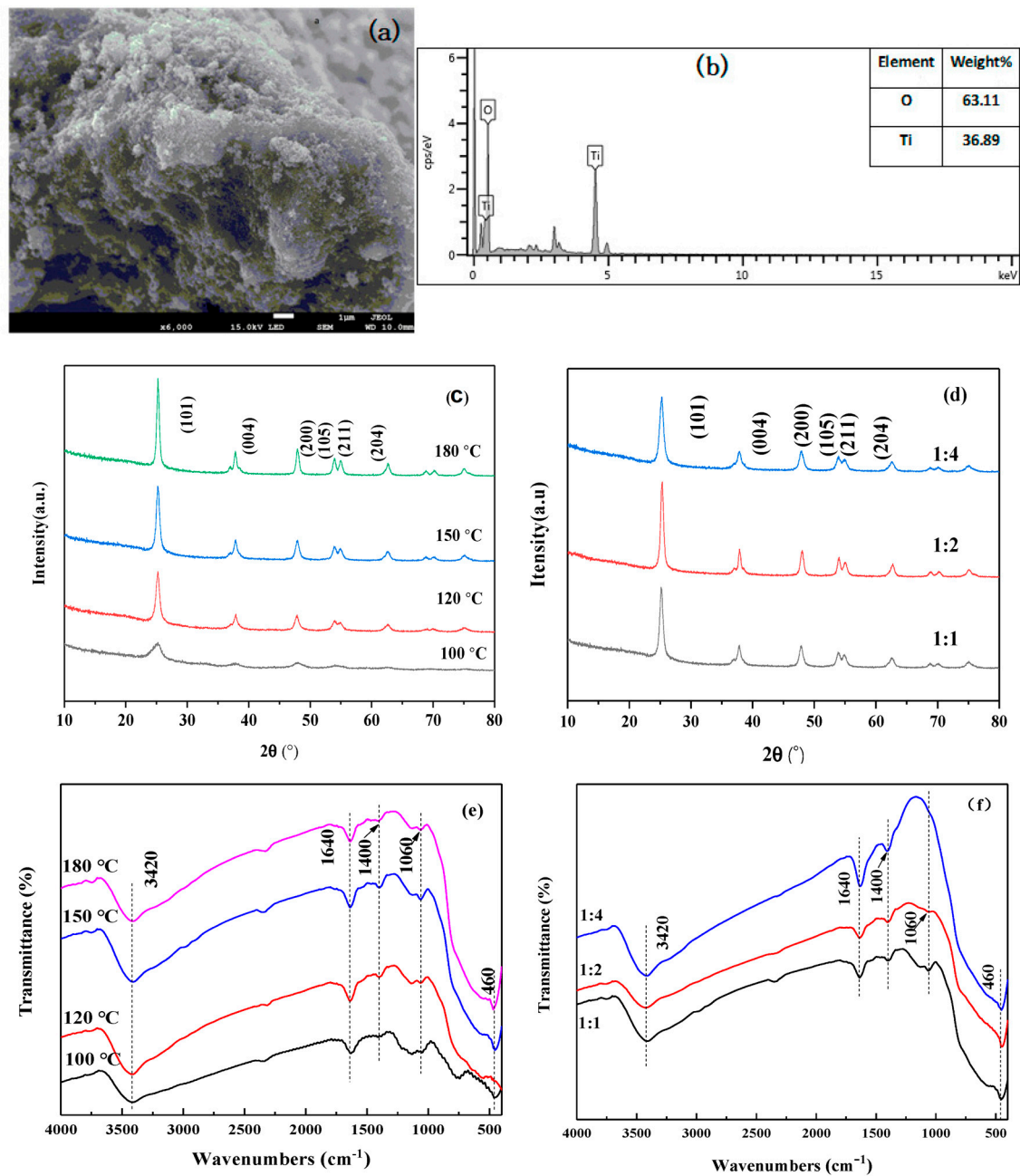


**Figure 4.** SEM images (a) and EDS elemental mapping analysis (b), XRD patterns (c,d), FTIR patterns (e,f) during TiO<sub>2</sub> nanoparticles.

### 3.2. Optimization of Photocatalytic Processes

The results of photocatalytic degradation of the landfill leachate by adjusting the irradiation time are shown in Figure 5a. During the dark reaction carried out for 30 min, the removal rates by TiO<sub>2</sub> adsorption of COD and color was 93.94% and 60%, respectively. The maximum COD and color removal rates were 89% and 70% under UV light, respectively. The reason for the increased COD value may be that the photocatalytic reaction oxidizes the complex macromolecular organics into small molecular organics after the light is turned on. Hassan et al. [37] pointed out that an increase in COD concentration at the end of photocatalysis is due to a decrease in catalytic efficiency caused by the deposition of pollutants on the catalyst with time. Sama Azadi et al. [38] also confirmed this conclusion. It is speculated that the reason for a COD removal rate that is higher than the chromaticity removal rate is due to low phenolic substances in the reaction process, as color reduction

simply reflects the oxidative opening benzene ring in the phenolic substances to other straight chain compounds [39]. The result is consistent with the removal rate of COD and color treated by AC/TiO<sub>2</sub> for the last 30 min [40]. The reason why the COD decrease was faster than the color removal needs more research. For this batch of the experiment, equal amounts of 200 mg TiO<sub>2</sub> were added into a series of test beakers containing 50 mL of the landfill leachate.

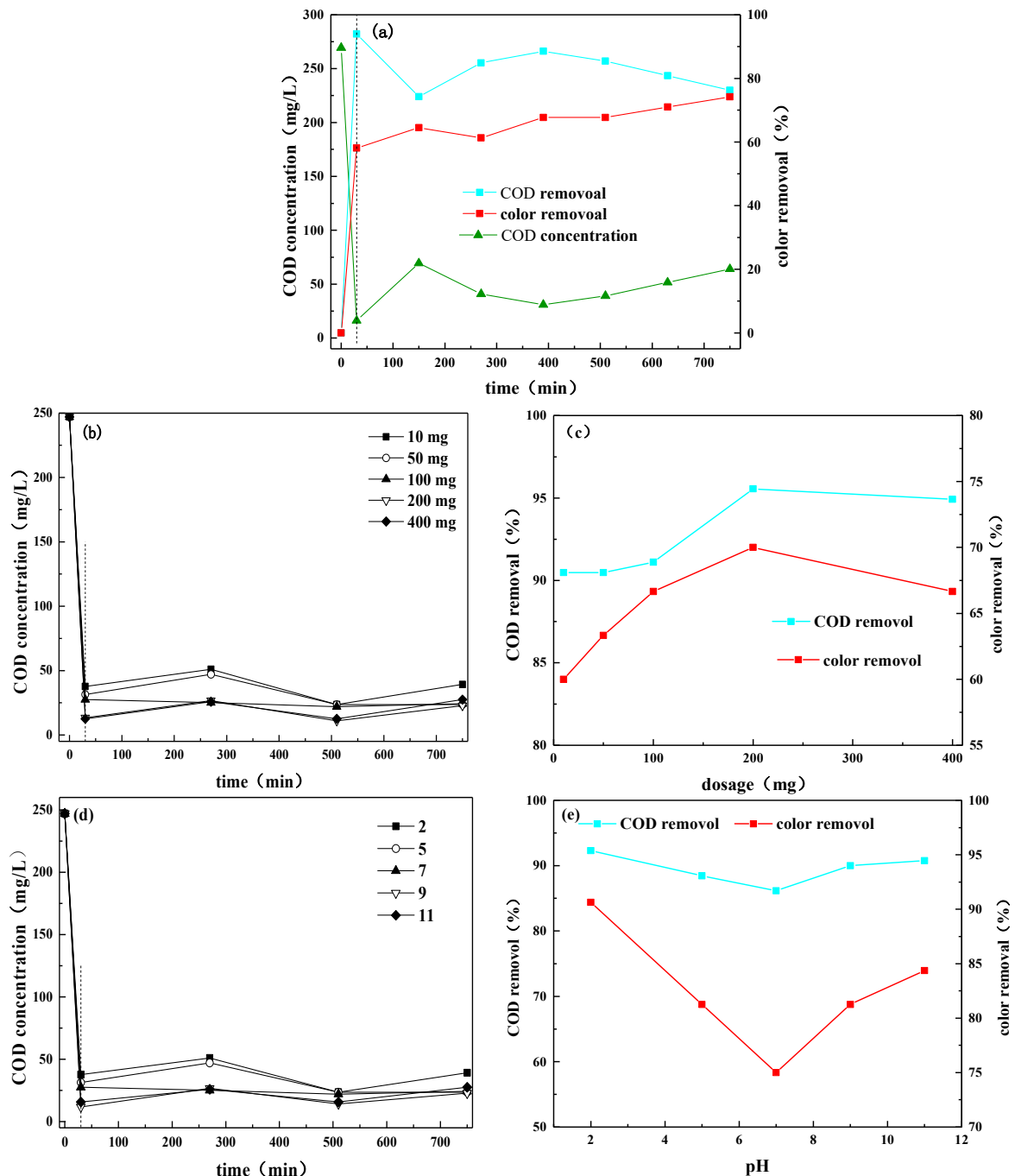


**Figure 5.** Effects of irradiation time (a), TiO<sub>2</sub> dosage (b,c) and initial pH (d,e) on COD concentration, removal and color removal.

As shown in Figure 5b,c, when the dosage of TiO<sub>2</sub> was 200 mg (4 g/L), the COD and decolorization removal rate were 94.28% and 70.00%, respectively. The highest photocatalytic efficiency did not appear at the dosage of 400 mg (8 g/L). The study confirmed that with the increase in the amount of TiO<sub>2</sub>, the irradiated area and the photocatalytic rate increased [41]. At a TiO<sub>2</sub> dosage of 4 g/L, Jia [42] removed 37.4% COD and 55.5% color, but the degradation ratio decreased, except COD, when the dosage was increased to 16 g/L. Miao et al. [43] noted that when the catalyst dosage reached the saturation level, the light absorption coefficient decreased. Therefore, the optimal dosage TiO<sub>2</sub> was 200 mg (4 g/L) in this study. For this batch of experiment, the duration of experiments performed was 750 min.

The results of photocatalytic degradation of the leachate at different initial pH values (2, 5, 7, 9, and 11) are shown in Figure 5d,e. During the reaction process, different pH values slightly affected the COD removal rate of approximately 85%. The color removal rate was evident under acidic conditions. When the pH value was 2, the color removal increased up to 87.5%. Jia et al. [44] studied the degradation of the landfill leachate by the photocatalytic treatment process and proposed that the optimal pH value was 4. Some researchers suggested that HCO<sub>3</sub><sup>-</sup>/CO<sub>3</sub><sup>2-</sup> anions brought about significant inhibitory effect on photocatalytic oxidation of refractory organics present in the leachate [45]. However, Xu et al. [46] noted that upon decreasing the leachate pH from 5.4 to 3.9, the amount and size of aggregated TiO<sub>2</sub> particles increased. Anpo and Kamat suggested that the highest pollutant adsorption and maximum photocatalytic removal efficiency were observed at a pH close to pH<sub>ZPC</sub> [47]. Azadi et al. [38] indicated that the pH<sub>ZPC</sub> values of C and C-W co-doped TiO<sub>2</sub> C-doped nanoparticles were 6.27 and 6.7, respectively, and the highest COD removal rate was in the range of pH value 6–7. The COD removal efficiency increased with leachate pH as reported in the literature [8]. Therefore, the pH value near pH<sub>ZPC</sub> had the best photocatalytic efficiency. In addition, the reason for the highest color removal rate at pH = 2 may be the conversion of colored substances to colorless substances during the photocatalytic reaction under strong acidity [48]. The original pH of the leachate in this test was alkaline (8.88), and the pH of the leachate was unadjusted from the engineering point of view. For this batch of the experiment, equal amounts of 200 mg TiO<sub>2</sub> were added into a series of test beakers containing 50 mL of the landfill leachate, and the duration of the experiments performed was 750 min.

In addition, combined with the maximum removal rates of COD and color under the three conditions, the optimal reaction time in this study was 500 min.

### 3.3. Treatment of Leachate by Aging Reactor Combined with Photocatalysis

The indicators of each reactor after acclimation are shown in Table 1.

**Table 1.** The indicators of each reactor after acclimation.

	NH <sub>4</sub> <sup>+</sup> -N (mg/L)	NO <sub>3</sub> -N (mg/L)	NO <sub>2</sub> -N (mg/L)	COD (mg/L)
C	5.457	18.209	0.079	245.302
D	1.049	18.226	0.017	185.955
E	18.404	8.5228	0.281	146.390
F	1.049	18.276	0.281	126.607

As shown in Figure 6a, from day 15 to 33, the concentrations of NH<sub>4</sub><sup>+</sup>-N in reactors D and F were 0.083–2.523 and 0.083–1.17 mg/L, respectively. The average removal rate was 80.3% for reactor D and 98.8% of reactor F. The NH<sub>4</sub><sup>+</sup>-N concentration in the effluent of the photocatalytic reaction was high, which was probably due to the photocatalytic reaction converting the nitrogen-containing organic matter into nitrogen-containing inorganic matter in the leachate. This finding shows that the leachate contains a large amount of heterocyclic nitrogen and amino compounds that readily hampered the nitrification–denitrification processes [9,49].

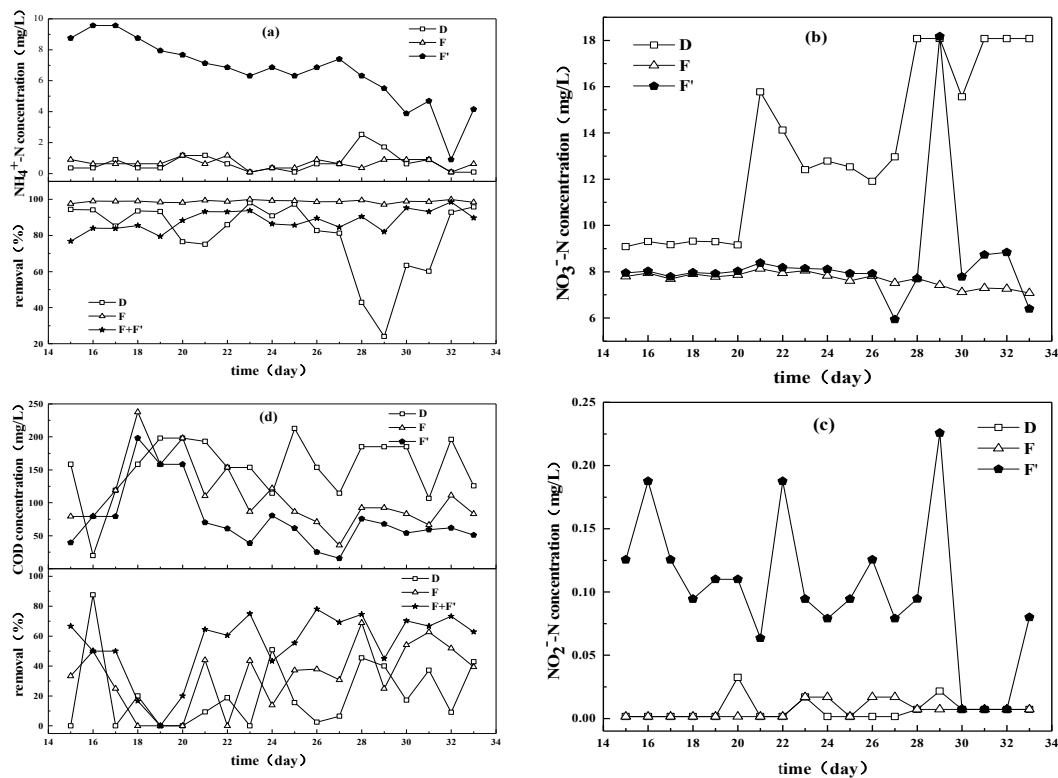
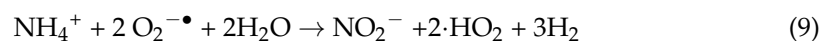


**Figure 6.** NH<sub>4</sub><sup>+</sup>-N concentration and removal (a), NO<sub>3</sub><sup>-</sup>-N concentration (b) NO<sub>2</sub><sup>-</sup>-N concentration (c), COD concentration and removal (d) of leachates.

Figure 6b illustrates that the concentration of NO<sub>3</sub>-N in the effluent of reactor D and the NO<sub>3</sub>-N concentration of the effluents of reactor F was 7–9 mg/L. Boonnorat et al. found that the leachate produced by a landfill for a long time contained low carbon/nitrogen (C/N) ratios [50]. The photocatalytic reaction of TiO<sub>2</sub> with a circulating leachate transformed the refractory organic matter into biodegradable organic matter, which was looped through the anaerobic landfill reactor E to accelerate the degradation of domestic waste and then recycled at the reactor F to provide a carbon source for denitrifying bacteria. Therefore, the concentration of NO<sub>3</sub><sup>-</sup>-N in reactor F was lower than that in reactor D [51,52]. Figure 6c shows that NO<sub>2</sub><sup>-</sup>-N concentrations of reactors D and F were 0.01–0.032 and 0.01–0.017 mg/L, respectively. However, the NO<sub>2</sub><sup>-</sup>-N concentration of the photocatalytic effluent F' increased, which confirms the conclusion that the nitrogen-containing organic matter shown in Figure 6a was degraded into NH<sub>4</sub><sup>+</sup>-N [53]. The N-compound conversion equation is as follows:



where  $\text{OH}^\bullet$  and  $\text{O}_2^{\bullet-}$  are active species produced in the photocatalytic process.

As shown in Figure 6d, at days 15 to 20, the COD concentration difference between the effluent of aged waste reactors D and F was not evident, and the microorganisms were still in a certain adaptation stage. From day 21 to the end of the process, the average COD removal rate (32.5%) of reactor F was also higher than that of reactor D (21.20%). At the end of the research, the COD concentrations of the effluent from reactor D and F were 125.49 and 83.14 mg/L, respectively; thus, reactor D satisfied the standard for pollution control on the landfill site of the MSW [28]. A possible explanation is that in the presence of organic compounds, the generated hydroxyl radicals interact with the aromatic and heterocyclic compounds present in the leachate, which favor the formation of small aliphatic chains of carboxylic acids resulting in compounds that are easily assimilated by microorganisms [54]. This result indicates that the photocatalytic reaction degrades the refractory organics into biodegradable organic matter, which can be degraded by the microorganisms in an aged waste reactor [55,56]. Accordingly, the photocatalytic reaction increases the biodegradable organic matter in the circulating leachate, which is more easily degraded by microorganisms in reactor F. With the combined process, it was possible to treat an effluent with a high organic load, meeting the restrictive standards of release in the recipient water bodies [57].

### 3.4. Photocatalyst Stability

The experiment of removing COD and color was repeated three times to evaluate the recycling and stability of the nanophotocatalyst. After each cycle, the catalyst was collected and washed by simple centrifugation, washed with deionized water, and dried at 120 °C. As shown in Figure 7, after three cycles, the COD removal rate was 90.00% and the color change rate was 63.33%. These findings indicate that after recovery, the nanophotocatalyst can maintain activity and continue to provide electrons during the photocatalytic reaction to promote substrate degradation. Therefore, it had good industrial application prospects.

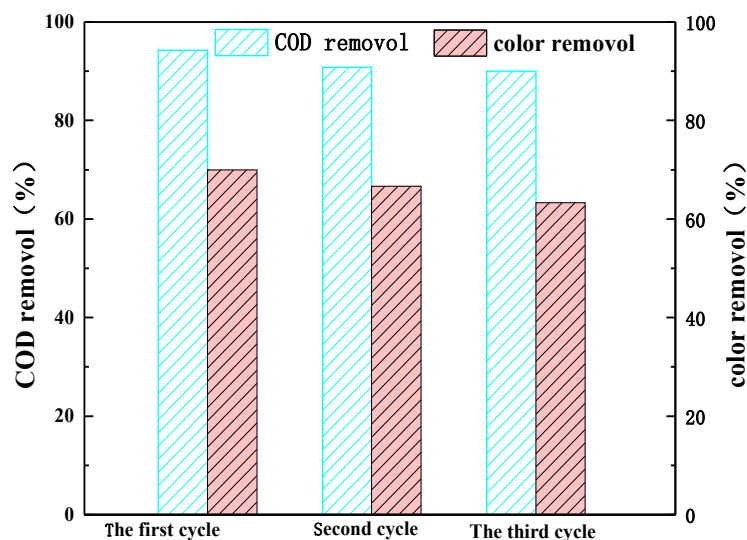
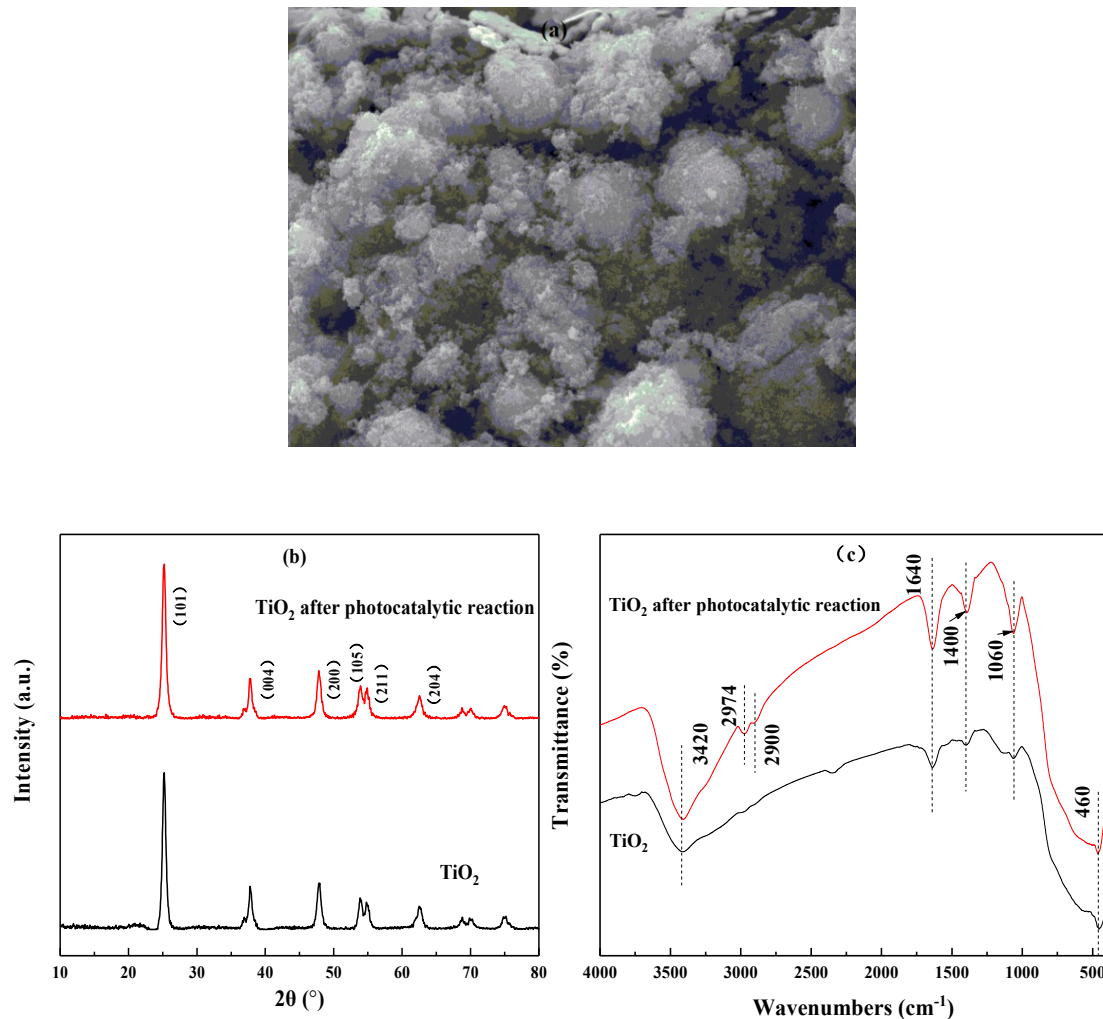


Figure 7.  $\text{TiO}_2$  recycling treatment effect.

XRD characterization, FTIR spectroscopy, SEM observation, and EDS analysis were carried out to study the structure, morphology, and chemical composition of the recovered  $\text{TiO}_2$  nanoparticles. As shown in Figure 8a, after the reaction, the  $\text{TiO}_2$  crystal form, crystal plane, and diffraction peak intensity did not significantly change. According to Scherrer's formula, the grain diameter after the reaction increased to 14.1 nm, but as the grain size increased, the specific surface area and the photocatalytic activity gradually decreased, consistent with the photocatalyst stability test results (Figure 8b). The FTIR diagram shows that, after the photocatalytic reaction, the characteristic peaks at 3420, 1640,

1400, and 1060  $\text{cm}^{-1}$  increased. This finding indicates that the surface of  $\text{TiO}_2$  adsorbed organic matter containing hydroxyl groups and  $\text{SO}_4^{2-}$ . In addition, the absorption peaks of CH and CO appeared at 2974  $\text{cm}^{-1}$  and 2900  $\text{cm}^{-1}$ , respectively, which was caused by the organic matter in the leachate that adsorbed on the surface of the  $\text{TiO}_2$  particles. However, the characteristic peak intensity of crystalline  $\text{TiO}_2$  molecules with a wavelength of 460  $\text{cm}^{-1}$  decreased. The reason may be that organic matter occupied the active site of  $\text{TiO}_2$ , thereby weakening the stretching of Ti–O and Ti–O–Ti vibration (Figure 8c). Accordingly,  $\text{TiO}_2$  nanoparticles have the potential to maintain high photocatalytic efficiency during stability tests.



**Figure 8.** SEM images (a), XRD patterns (b) and FTIR patterns (c) of  $\text{TiO}_2$  nanoparticles before and after photocatalysis.

#### 4. Conclusions

The effects of  $\text{TiO}_2$  nanoparticles and aged waste reactor combined treatment of  $\text{NH}_4^+$ -N,  $\text{NO}_3^-$ -N,  $\text{NO}_2^-$ -N, and COD in landfill leachate were discussed. SEM, FTIR, and XRD were used to determine the optimal hydrothermal reaction temperature of the synthesized nanoparticles at 150  $^\circ\text{C}$ , and the ratio of titanium to urea was 1:1. Then, considering the removal rate for COD and chromaticity as the index, the optimal photocatalytic reaction time was 500 min, the best dosage of  $\text{TiO}_2$  nanoparticles was 4 g/L, and the original leachate had pH = 8.88. The removal rates of COD and chroma under three conditions were obtained by the single-factor control method: 89% and 70%; 95.56% and 70%; and 85% and 87.5%, respectively. Under the best process conditions, after the combined treatment with  $\text{TiO}_2$  nanoparticles and an aged waste reactor for landfill leachate, the overall average removal

rates of  $\text{NH}_4^+\text{-N}$  and COD were 98.8% and 32.5%, respectively. The concentration of  $\text{NO}_3^-\text{-N}$  and  $\text{NO}_2^-\text{-N}$  were maintained at 7–9 and 0.01–0.017 mg/L, respectively. The combined device degraded the refractory biodegradable organic matter into biodegradable organic matter, and the recharge to the anaerobic bioreactor landfill can continue to accelerate the degradation of domestic garbage. This simulation of photocatalysis-landfilling could be a baseline study for the implementation of technology at the pilot scale to accelerate the process of waste stabilization.

**Author Contributions:** Conceptualization, C.W.; data curation, C.W. and H.S.; funding acquisition, X.S.; investigation, B.X., H.Z.; methodology, H.S.; project administration, B.X.; software, C.W.; supervision, X.S.; writing—original draft, C.W.; writing—review and editing, X.S. and H.Z. All authors have read and agreed to the published version of the manuscript.

**Funding:** This research was funded by National Natural Science Foundation of China (No. 52070049); Natural Science Foundation of Guangxi (No. 2018GXNSFGA281001); Science and Technology Major Project of Guangxi (GuikeAA18118013); Innovation Project of Guangxi Graduate Education (No. YCSW2021198).

**Institutional Review Board Statement:** Not applicable.

**Informed Consent Statement:** Not applicable.

**Data Availability Statement:** The data presented in this study are available on request from the authors.

**Conflicts of Interest:** The authors declare no conflict of interest.

## References

1. Guo, Y.; Sheehan, J.D.; Chen, Z.; Wang, S. Oxidative degradation of landfill leachate by catalysis of  $\text{CeMnOx}/\text{TiO}_2$  in super-critical water: Mechanism and kinetic study. *Chem. Eng. J.* **2018**, *578*–586.
2. Yang, Y.; Liu, Z.; Demeestere, K.; Van Hulle, S. Ozonation in view of micropollutant removal from biologically treated landfill leachate: Removal efficiency, OH exposure, and surrogate-based monitoring. *Chem. Eng. J.* **2021**, *410*, 128413. [[CrossRef](#)]
3. Clarke, B.O.; Anumol, T.; Barlaz, M.; Snyder, S.A. Investigating landfill leachate as a source of trace organic pollutants. *Chemosphere* **2015**, *127*, 269–275. [[CrossRef](#)] [[PubMed](#)]
4. Gao, J.; Oloibiri, V.; Chys, M.; Audenaert, W.T.M.; Decostere, B.; He, Y.; Van Langenhove, H.; Demeestere, K.; Van Hulle, S.W.H. The present status of landfill leachate treatment and its development trend from a technological point of view. *Rev. Environ. Sci. Biol. Technol.* **2015**, *14*, 93–122. [[CrossRef](#)]
5. Duyar, A.; Ciftcioglu, V.; Cirik, K.; Civelekoglu, G.; Uruş, S. Treatment of landfill leachate using single-stage anoxic moving bed biofilm reactor and aerobic membrane reactor. *Sci. Total. Environ.* **2021**, *776*, 145919. [[CrossRef](#)] [[PubMed](#)]
6. Luo, H.; Zeng, Y.; Cheng, Y.; He, D.; Pan, X. Recent advances in municipal landfill leachate: A review focusing on its characteristics, treatment, and toxicity assessment. *Sci. Total. Environ.* **2020**, *703*, 135468. [[CrossRef](#)] [[PubMed](#)]
7. Hassan, M.; Xie, B. Use of aged refuse-based bioreactor/biofilter for landfill leachate treatment. *Appl. Microbiol. Biotechnol.* **2014**, *98*, 6543–6553. [[CrossRef](#)]
8. Chys, M.; Oloibiri, V.A.; Audenaert, W.T.; Demeestere, K.; Van Hulle, S.W. Ozonation of biologically treated landfill leachate: Efficiency and insights in organic conversions. *Chem. Eng. J.* **2015**, *277*, 104–111. [[CrossRef](#)]
9. Oloibiri, V.; Chys, M.; De Wandel, S.; Demeestere, K.; Van Hulle, S.W. Removal of organic matter and ammonium from landfill leachate through different scenarios: Operational cost evaluation in a full-scale case study of a Flemish landfill. *J. Environ. Manag.* **2017**, *203*, 774–781. [[CrossRef](#)] [[PubMed](#)]
10. Chen, W.; Gu, Z.; Wen, P.; Li, Q. Degradation of refractory organic contaminants in membrane concentrates from landfill leachate by a combined coagulation-ozonation process. *Chemosphere* **2019**, *217*, 411–422. [[CrossRef](#)]
11. Chys, M.; Declerck, W.; Audenaert, W.T.; Van Hulle, S. UV/ $\text{H}_2\text{O}_2$ ,  $\text{O}_3$  and (photo-) Fenton as treatment prior to granular activated carbon filtration of biologically stabilized landfill leachate. *J. Chem. Technol. Biotechnol.* **2014**, *90*, 525–533. [[CrossRef](#)]
12. Xu, Q.; Tian, Y.; Wang, S.; Ko, J.H. A comparative study of leachate quality and biogas generation in simulated anaerobic and hybrid bioreactors. *Waste Manag.* **2015**, *41*, 94–100. [[CrossRef](#)]
13. Li, J.; Wu, B.; Li, Q.; Zou, Y.; Cheng, Z.; Sun, X.; Xi, B. Ex situ simultaneous nitrification-denitrification and in situ denitrification process for the treatment of landfill leachates. *Waste Manag.* **2019**, *88*, 301–308. [[CrossRef](#)] [[PubMed](#)]
14. Xu, Q.; Siracusa, G.; Di Gregorio, S.; Yuan, Q. COD removal from biologically stabilized landfill leachate using Advanced Oxidation Processes (AOPs). *Process Saf. Environ. Protect.* **2018**, *120*, 278–285. [[CrossRef](#)]
15. Fresno, F.; Portela, R.; Suárez, S.; Coronado, J.M. Photocatalytic materials: Recent achievements and near future trends. *J. Mater. Chem. A* **2014**, *2*, 2863–2884. [[CrossRef](#)]
16. Yan, M.; Wu, Y.; Liu, X. Photocatalytic nanocomposite membranes for high-efficiency degradation of tetracycline under visible light: An imitated core-shell Au-TiO<sub>2</sub>-based design. *J. Alloys Compd.* **2021**, *855*, 157548. [[CrossRef](#)]

17. Chen, J.; Xiong, Y.; Duan, M.; Li, X.; Li, J.; Fang, S.W.; Qin, S.; Zhang, R. Insight into the Synergistic Effect of Adsorption-Photocatalysis for the Removal of Organic Dye Pollutants by Cr-Doped ZnO. *Langmuir* **2020**, *36*, 520–533. [[CrossRef](#)] [[PubMed](#)]
18. Mirzaei, M.; Dabi, B.; Dadvar, M.; Jafarikojour, M. Photocatalysis of Phenol Using a Spinning Disc Photoreactor Immobilized with TiO<sub>2</sub> Nanoparticles: Hydrodynamic Modeling and Reactor Optimization. *Ind. Eng. Chem. Res.* **2017**, *56*, 1739–1749. [[CrossRef](#)]
19. Yu, X.; Qiu, H.; Wang, B.; Meng, Q.; Zhao, K. A ternary photocatalyst of all-solid-state Z-scheme TiO<sub>2</sub>-Au-BiOBr for efficiently degrading various dyes. *J. Alloys Compd.* **2020**, *839*, 155597. [[CrossRef](#)]
20. Altina, I.; Mab, X.; Boffab, V.; Bacakszic, E.; Magnaccad, G. Hydrothermal preparation of B-TiO<sub>2</sub>-graphene oxide ternary nanocomposite, characterization and photocatalytic degradation of bisphenol A under simulated solar irradiation. *Mater. Sci. Semicond. Process.* **2021**, *123*, 105591. [[CrossRef](#)]
21. Shao, S.; Yu, J.; Love, J.B.; Fan, X. An economic approach to produce iron doped TiO<sub>2</sub> nanorods from ilmenite for photocatalytic applications. *J. Alloys Compd.* **2021**, *858*, 158388. [[CrossRef](#)]
22. Priyanka, K.; Remya, N.; Behera, M. Comparison of titanium dioxide based catalysts preparation methods in the mineralization and nutrients removal from greywater by solar photocatalysis. *J. Clean Prod.* **2019**, *235*, 1–10. [[CrossRef](#)]
23. Seibert, D.; Borba, F.H.; Bueno, F.; Inticher, J.J.; Modenes, A.N.; Espinoza-Quinones, F.R.; Bergamasco, R. Two-stage integrated system photo-electro-Fenton and biological oxidation process assessment of sanitary landfill leachate treatment: An intermediate products study. *Chem. Eng. J.* **2019**, *372*, 471–482. [[CrossRef](#)]
24. Cai, F.F.; Yang, Z.H.; Huang, J.; Zeng, G.M.; Wang, L.K.; Yang, J. Application of cetyltrimethylammonium bromide bentonite-titanium dioxide photocatalysis technology for pretreatment of aging leachate. *J. Hazard. Mater.* **2014**, *275*, 63–71. [[CrossRef](#)] [[PubMed](#)]
25. Pellenz, L.; Borba, F.H.; Daroit, D.J.; Lassen, M.F.M.; Baroni, S.; Zorzo, C.F.; Guimarães, R.E.; Espinoza-Quinones, F.R.; Seibert, D. Landfill leachate treatment by a boron-doped diamond-based photo-electro-Fenton system integrated with biological oxidation: A toxicity, genotoxicity and by products assessment. *J. Environ. Manag.* **2020**, *264*, 110473. [[CrossRef](#)]
26. Gu, Z.; Chen, W.; Wang, F.; Li, Q. A pilot-scale comparative study of bioreactor landfills for leachate decontamination and municipal solid waste stabilization. *Waste Manag.* **2020**, *103*, 113–121. [[CrossRef](#)]
27. Agdag, O.N.; Aktas, D.; Simsek, O. Effects of Different Seed Substances on Anaerobic Degradation of Municipal Solid Waste in Recirculated Bioreactor. *Waste Biomass-Valoriz.* **2021**, *12*, 383–392. [[CrossRef](#)]
28. Ministry of Environmental Protection of the People's Republic of China. *Standard for pollution control on the landfill site of the MSW*; Ministry of Environmental Protection of the People's Republic of China: Beijing, China, 2008.
29. Wu, C.; Shen, L.; Zhang, Y.-C.; Huang, Q. Solvothermal synthesis of Cr-doped ZnO nanowires with visible light-driven photocatalytic activity. *Mater. Lett.* **2011**, *65*, 1794–1796. [[CrossRef](#)]
30. Sun, X.; Zhang, H.; Cheng, Z. Use of bioreactor landfill for nitrogen removal to enhance methane production through ex situ simultaneous nitrification-denitrification and in situ denitrification. *Waste Manag.* **2017**, *66*, 97–102. [[CrossRef](#)]
31. He, J.; Yang, J.; Jiang, F.; Liu, P.; Zhu, M. Photo-assisted peroxydisulfate activation via 2D/2D heterostructure of Ti<sub>3</sub>C<sub>2</sub>/g-C<sub>3</sub>N<sub>4</sub> for degradation of diclofenac. *Chemosphere* **2020**, *258*, 127339. [[CrossRef](#)]
32. Elleuch, L.; Messaoud, M.; Djebali, K.; Attafi, M.; Cherni, Y.; Kasmi, M.; Elaoud, A.; Trabelsi, I.; Chatti, A. A new insight into highly contaminated landfill leachate treatment using Kefir grains pre-treatment combined with Ag-doped TiO<sub>2</sub> photocatalytic process. *J. Hazard. Mater.* **2020**, *382*, 121119. [[CrossRef](#)]
33. Ebrahimian, A. Silver Doped TiO<sub>2</sub> Nanoparticles: Preparation, Characterization and Efficient Degradation of 2,4-dichlorophenol Under Visible Light. *J. Water Environ. Nanotechnol.* **2016**, *1*, 135–144.
34. Xu, C.; Yang, F.; Deng, B.; Zhuang, Y.; Li, D.; Liu, B.; Yang, W.; Li, Y. Ti<sub>3</sub>C<sub>2</sub>/TiO<sub>2</sub> nanowires with excellent photocatalytic performance for selective oxidation of aromatic alcohols to aldehydes. *J. Catal.* **2020**, *383*, 1–12. [[CrossRef](#)]
35. Peng, C.; Wang, H.; Yu, H.; Peng, F. (111) TiO<sub>2</sub>-x/Ti<sub>3</sub>C<sub>2</sub>: Synergy of active facets, interfacial charge transfer and Ti<sup>3+</sup> doping for enhance photocatalytic activity. *Mater. Res. Bull.* **2017**, *89*, 16–25. [[CrossRef](#)]
36. Lv, K.; Zuo, H.; Sun, J.; Deng, K.; Liu, S.; Li, X.; Wang, D. (Bi, C and N) codoped TiO<sub>2</sub> nanoparticles. *J. Hazard. Mater.* **2009**, *161*, 396–401. [[CrossRef](#)]
37. Hassan, M.; Zhao, Y.; Xie, B. Employing TiO<sub>2</sub> photocatalysis to deal with landfill leachate: Current status and development. *Chem. Eng. J.* **2016**, *285*, 264–275. [[CrossRef](#)]
38. Azadi, S.; Karimi-Jashni, A.; Javadpour, S.; Amiri, H. Photocatalytic treatment of landfill leachate: A comparison between N-, P-, and N-P-type TiO<sub>2</sub> nanoparticles. *Environ. Technol. Innov.* **2020**, *19*, 100985. [[CrossRef](#)]
39. Qazaq, A.; Hudaya, T.; Lee, I.; Sulidis, A.; Adesina, A. Photoremediation of natural leachate from a municipal solid waste site in a pilot-scale bubble column reactor. *Catal. Commun.* **2007**, *8*, 1917–1922. [[CrossRef](#)]
40. Rojviroon, O.; Rojviroon, T.; Sirivithayapakorn, S. Removal of Color and Chemical Oxygen Demand from Landfill Leachate by Photocatalytic Process with AC/TiO<sub>2</sub>. *Energy Procedia* **2015**, *79*, 536–541. [[CrossRef](#)]
41. Jyothi, K.; Yesodharan, S.; Yesodharan, E. Ultrasound (US), Ultraviolet light (UV) and combination (US + UV) assisted semiconductor catalysed degradation of organic pollutants in water: Oscillation in the concentration of hydrogen peroxide formed in situ. *Ultrason. Sonochem.* **2014**, *21*, 1787–1796. [[CrossRef](#)]
42. Youngman, F. Optimization of TiO<sub>2</sub> Photocatalyst in an Advanced Oxidation Process for the Treatment of Landfill Leachate. Ph.D. Thesis, Florida Atlantic University, Boca Raton, FL, USA, 2013.

43. Miao, Z.; Wang, G.; Li, L.; Wang, C.; Zhang, X. Fabrication of black TiO<sub>2</sub>/TiO<sub>2</sub> homojunction for enhanced photocatalytic degradation. *J. Mater. Sci.* **2019**, *54*, 14320–14329. [[CrossRef](#)]
44. Jia, C.; Wang, Y.; Zhang, C.; Qin, Q. UV-TiO<sub>2</sub> Photocatalytic Degradation of Landfill Leachate. *Water Air Soil Pollut.* **2011**, *217*, 375–385. [[CrossRef](#)]
45. Wiszniowski, J.; Robert, D.; Surmacz-Górska, J.; Miksch, K.; Malato, S.; Weber, J.-V. Solar photocatalytic degradation of humic acids as a model of organic compounds of landfill leachate in pilot-plant experiments: Influence of inorganic salts. *Appl. Catal. B Environ.* **2004**, *53*, 127–137. [[CrossRef](#)]
46. He, X.; Mitrano, D.M.; Nowack, B.; Bahk, Y.K.; Figi, R.; Schreiner, C.; Bürki, M.; Wang, J. Agglomeration potential of TiO<sub>2</sub> in synthetic leachates made from the fly ash of different incinerated wastes. *Environ. Pollut.* **2017**, *223*, 616–623. [[CrossRef](#)] [[PubMed](#)]
47. Anpo, M.; Kamat, P.V. *Environmentally Benign Photocatalysts*; Springer: New York, NY, USA, 2010.
48. Chen, C.-Y. Photocatalytic Degradation of Azo Dye Reactive Orange 16 by TiO<sub>2</sub>. *Water Air Soil Pollut.* **2009**, *202*, 335–342. [[CrossRef](#)]
49. Hassan, M.; Wang, X.; Wang, F.; Wu, D.; Hussain, A.; Xie, B. Coupling ARB-based biological and photochemical (UV/TiO<sub>2</sub> and UV/S<sub>2</sub>O<sub>8</sub><sup>2-</sup>) techniques to deal with sanitary landfill leachate. *Waste Manag.* **2017**, *63*, 292–298. [[CrossRef](#)]
50. Boonnorat, J.; Honda, R.; Panichnumsin, P.; Boonapatcharoen, N.; Yenjam, N.; Krasaesueb, C.; Wachirawat, M.; Seemuang-On, S.; Jutakanoke, R.; Teeka, J.; et al. Treatment efficiency and greenhouse gas emissions of non-floating and floating bed activated sludge system with acclimatized sludge treating landfill leachate. *Bioresour. Technol.* **2021**, *330*, 124952. [[CrossRef](#)]
51. Guo, X.; Li, B.; Zhao, R.; Zhang, J.; Lin, L.; Zhang, G.; Li, R.-H.; Liu, J.; Li, P.; Li, Y.; et al. Performance and bacterial community of moving bed biofilm reactors with various biocarriers treating primary wastewater effluent with a low organic strength and low C/N ratio. *Bioresour. Technol.* **2019**, *287*, 121424. [[CrossRef](#)] [[PubMed](#)]
52. Gomes, A.I.; Foco, M.L.; Vieira, E.; Cassidy, J.; Silva, T.F.; Fonseca, A.; Saraiva, I.; Boaventura, R.A.; Vilar, V.J. Multistage treatment technology for leachate from mature urban landfill: Full scale operation performance and challenges. *Chem. Eng. J.* **2019**, *376*, 120573. [[CrossRef](#)]
53. Gogina, E.; Gulshin, I. Simultaneous Nitrification and Denitrification with Low Dissolved Oxygen Level and C/N ratio. *Procedia Eng.* **2016**, *153*, 189–194. [[CrossRef](#)]
54. Liu, T.; He, X.; Jia, G.; Xu, J.; Quan, X.; You, S. Simultaneous nitrification and denitrification process using novel surface-modified suspended carriers for the treatment of real domestic wastewater. *Chemosphere* **2020**, *247*, 125831. [[CrossRef](#)] [[PubMed](#)]
55. Gomes, A.I.; Soares, T.F.; Silva, T.F.; Boaventura, R.A.; Vilar, V.J. Ozone-driven processes for mature urban landfill leachate treatment: Organic matter degradation, biodegradability enhancement and treatment costs for different reactors configuration. *Sci. Total. Environ.* **2020**, *724*, 138083. [[CrossRef](#)] [[PubMed](#)]
56. Abu Amr, S.S.; Aziz, H.A.; Adlan, M.N.; Aziz, S.Q. Effect of Ozone and Ozone/Fenton in the Advanced Oxidation Process on Biodegradable Characteristics of Semi-aerobic Stabilized Leachate. *Clean-Soil Air Water* **2012**, *41*, 148–152. [[CrossRef](#)]
57. Colombo, A.; Módenes, A.N.; Trigueros, D.E.G.; da Costa, S.I.G.; Borba, F.; Espinoza-Quiñones, F.R. Treatment of sanitary landfill leachate by the combination of photo-Fenton and biological processes. *J. Clean. Prod.* **2019**, *214*, 145–153. [[CrossRef](#)]